Dalton Transactions

PAPER

View Article Online
View Journal | View Issue

Cite this: *Dalton Trans.*, 2018, **47**, 9459

Confinement of H_2O and EtOH to enhance CO_2 capture in MIL-53(Al)-TDC†

Gerardo A. González-Martínez, ‡[a] Tamara Jurado-Vázquez,‡[a] Diego Solís-Ibarra, *[a] Brenda Vargas,[a] Elí Sánchez-González, [a] Ana Martínez,[b] Rubicelia Vargas, [c] Eduardo González-Zamora *[c] and Ilich A. Ibarra *[a]

Received 8th April 2018,
Accepted 19th June 2018

DOI: 10.1039/c8dt01369a

rsc.li/dalton

EtOH sorption properties were investigated in MIL-53(Al)-TDC and found a strong interaction between EtOH and the MOF material (ΔH_{ads} = 69.6 kJ mol^{-1}). CO_2 capture was enhanced upon confining small amounts of H_2O. Upon confining small amounts of EtOH however, the CO_2 uptake was not improved. The difference in CO_2 uptake with EtOH and H_2O was rationalised using computational calculations. The analysis of the quantum theory of atoms in molecules (QTAIM) showed a covalent interaction between a MOF model and confined molecules (EtOH and H_2O), and no difference in the hydrogen bonds between confined molecules and CO_2.

Introduction

The properties of porous materials have been extensively studied in the past few years due to their potential applications to solve environmental problems. Among this group of materials, metal–organic frameworks (MOFs) are a very promising subgroup of porous materials due to their tuneable chemical composition. MOFs have been defined as crystalline materials consisting of metal ions and organic bridging ligands with potential voids.[1] One of the current environmental problems that has attracted special attention is the increase of carbon dioxide (CO_2) concentrations in the atmosphere, due to emissions produced by the combustion of fossil fuels. The direct consequence is the worldwide temperature increase of 0.78 °C since the Industrial Revolution until now.[2] Particularly, in 2017 the worldwide CO_2 emissions increased approximately 2% in comparison with the 2014–2016 period. This increment meant a record of 36.8 Gt of CO_2 reached in the atmosphere.[3] Recently Poliakoff[4] elegantly proposed, among the 12 principles of CO_2 chemistry, the relevance of maximising the integration of separation and utilization of CO_2. For example, CO_2 can be re-used in some catalytic transformations, like Fischer–Tropsch synthesis,[5] to produce hydrocarbons. The use of MOFs for these tasks represents a very promising alternative. In particular, MOFs have exhibited a high structural stability, adsorption capacity and mild regeneration conditions for CO_2 capture and separation.[6] Typically, the enhancement of CO_2 capture in these materials has been achieved by the improvement of host–guest interactions. Thus, the use of different synthetic strategies that involve functionalisation of the pores with Lewis basic groups (*e.g.*, amines[7]), and the generation of open metal sites,[8] Lewis acid sites, have been successfully demonstrated to enhance CO_2 interactions with MOF materials. A new and exciting strategy to improve CO_2 capture is the confinement of solvents in MOFs. In general, the confinement of solvents within porous materials generates several modifications on the physical properties of these solvents (*e.g.* viscosity, density, dielectric constant and specific heat) and the absorptive properties of the host material.[9] Remarkable examples, on this technology, were presented by Llewellyn,[10] Walton[11] and Qian.[12] In our group, we are interested in studying and developing hybrid MOF materials to sequester large amounts of CO_2 by the confinement of polar solvents inside their micropores (bottleneck effect[13]). Previously, we have investigated the enhancement of CO_2 capture *via* confining small amounts of DMF,[14] MeOH,[15] EtOH,[13] i-PrOH,[15b] *n*-PrOH[16] and H_2O,[17] in hydroxo (μ_2-OH) functionalised MOFs.

Our group is particularly interested in the hydroxo-functionalised material MIL-53(Al) due to the great accessibility for its

[a]*Laboratorio de Fisicoquímica y Reactividad de Superficies (LaFReS), Instituto de Investigaciones en Materiales, Universidad Nacional Autónoma de México, Circuito Exterior s/n, CU, Del. Coyoacán, 04510, Ciudad de México, Mexico. E-mail: argel@unam.mx, dgo.solis@gmail.com*

[b]*Instituto de Investigaciones en Materiales, Universidad Nacional Autónoma de México, Circuito Exterior s/n, CU, Del. Coyoacán, 04510, Ciudad de México, Mexico*

[c]*Departamento de Química, Universidad Autónoma Metropolitana-Iztapalapa, San Rafael Atlixco 186, Col. Vicentina, Iztapalapa, C. P. 09340, Ciudad de México, Mexico. E-mail: egz@xanum.uam.mx; Fax: +52(55) 5622-4595*

†Electronic supplementary information (ESI) available: Dynamic CO_2 capture, dynamic CO_2 capture under humid conditions, loading of small amounts of EtOH (activation protocol) and computational details. See DOI: 10.1039/c8dt01369a

‡These authors contributed equally to this work.

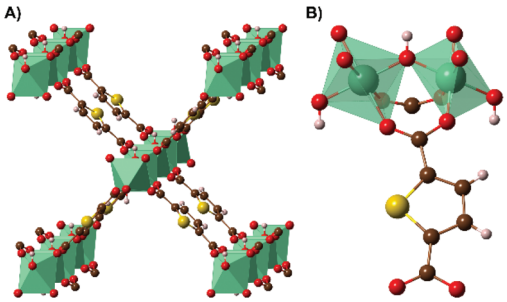

Fig. 1 Schematic representation of: (A) crystal structure of MIL-53(Al) TDC and (B) view of the binuclear building block of two metal ion oxygen octahedra bridged by a μ_2-hydroxo group.

synthesis (*e.g.*, relatively cheap starting materials and short reaction times). Previously, we studied the effect of confining small H_2O molecules within MIL-53(Al) to increase its CO_2 capture adsorption properties.[17a] MIL-53(Al) showed a CO_2 capture of 3.5 wt% (CO_2 kinetic uptake experiments, under anhydrous conditions, at 303 K). Upon confining small amounts of water, a 1.5-fold increase in the CO_2 capture was observed (5.2 wt%).[17a] Additionally, we reported the effect of including an extra hydrophilic functional group (NH_2) on the CO_2 capture, under humid conditions, on NH_2-MIL-53(Al).[17b] Thus, any analogue to MIL-53(Al) is of great interest to us.

Recently, Stock *et al.*[18] reported the synthesis of an isoreticular MIL-53(Al) network denominated MIL-53(Al)-TDC. This microporous Al(III)-MOF material is constructed with the 2,5-thiophenedicarboxylate (TDC) ligand instead of the traditional 1,4-benzendicarboxylate (BDC) reported by Loiseau *et al.*[19] MIL-53(Al)-TDC crystallised in the *Pmna* space group and showed a characteristic [$Al_2(\mu_2$-OH)] building block. Each Al(III) centre adopted an octahedral geometry with four oxygen donors from four different TDC ligands and two hydroxo (μ_2-OH) groups (Fig. 1). These connections lead to square shape channels of approximately 8 Å per side. Herein, we report the CO_2 capture enhancement (by confining small amounts of H_2O) in the material MIL-53(Al)-TDC.

Experimental

Synthesis of MIL-53(Al)-TDC

The synthesis of MIL-53(Al)-TDC was based on a method previously reported by Stock *et al.*[18] and modified as follows: 64 mg of $AlCl_3$ (Reagent Plus Sigma Aldrich, 99%) and 62 mg of 2,5-thiophenedicarboxilic acid were mixed in 1.8 mL of DMF and 2.5 mL of H_2O. This mixture was heated at 100 °C for 5 hours in a pressure tube of 20 mL. After the reaction was completed and cooled down to room temperature, the product was filtered under vacuum and washed with DMF (5 mL). To remove the excess of ligand inside the MOF material, the as-synthesised product was then mixed with DMF and heated to 150 °C for 1 h. To remove DMF molecules from its pores, samples of DMF treated MIL-53(Al)-TDC were acetone-exchanged. Then, an acetone-exchanged sample was activated at 200 °C for 4 hours under vacuum and a N_2 adsorption isotherm was performed (77 K) and its BET surface area was determined ($0.01 < P/P_0 < 0.04$) to be 1443 $m^2\ g^{-1}$.

Adsorption isotherms for N_2, H_2O and EtOH

N_2 isotherms (up to 1 bar and 77 K) was recorded on a Belsorp mini II analyser under high vacuum in a clean system with a diaphragm pumping system. H_2O and EtOH sorption isotherms were measured at 30 °C using a gravimetric method in a DVS Advantage 1 from Surface Measurement System, UK. This instrument consists of a Cahn microbalance (mass sensitivity: 0.1 μg), with a digital optical microscope, set in an exactly controlled temperature and vapour pressure chamber (accuracy: 0.1 K and 0.7% P/P_0, respectively). Dry, high-purity nitrogen was used as a carrier gas.

PXRD experiments

Powder X-ray diffraction (PXRD) patterns were collected in Bragg–Brentano geometry with Cu-$K_{\alpha 1}$ radiation (λ = 1.540562 Å) in a Rigaku ULTIMA IV with a nickel filter. The powder patterns were recorded from 5 to 40° (2θ) in 0.01° steps and at a scan rate of 0.319° min^{-1}.

CO_2 capture experiments

Kinetic uptake experiments were conducted using a thermobalance (Q500 HR, TA Instruments) at 30 °C with a constant CO_2 gas flow rate of 60 mL min^{-1} (see the ESI†). Water co-adsorption followed by CO_2 adsorption experiments were carried out using a dynamic water vapour sorption analyser (Q5000 SA, TA Instruments) at 30 °C with a constant CO_2 flow (60 mL min^{-1}) on activated samples (180 °C for 1 h and under vacuum) of MIL-53(Al)-TDC.

Results and discussion

CO_2 capture experiments

Dynamic CO_2 adsorption experiments were performed on the acetone-exchanged samples of MIL-53(Al)-TDC (*vide supra*). First, an acetone-exchanged sample of MIL-53(Al)-TDC was placed inside a thermobalance and activated by heating from room temperature up to 200 °C for 1 h and under a flow of pure N_2 gas. Then, the activated sample was cooled down to 30 °C (under N_2). Then, the N_2 flow was switched to 60 mL min^{-1} of CO_2. At this temperature, the material showed a maximum weight percentage gain, which indicated the maximum amount of CO_2 captured. This amount corresponds to 5.0 wt%, which was rapidly reached after only 4 minutes and remained constant until the end of the experiment, 15 minutes, (see Fig. 2, top).

Later, an acetone-exchanged sample of MIL-53(Al)-TDC was placed into a humidity-controlled thermobalance and activated as before (200 °C for 1 h). After the sample had reached 30 °C, the equipment was allowed to stabilise at 10%RH (small

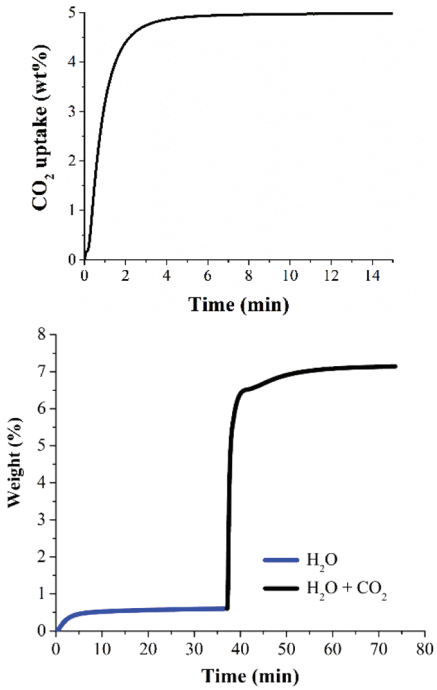

Fig. 2 Kinetic CO_2 uptake experiments, carried out at 30 °C, of (top) anhydrous CO_2 and (bottom) 10% RH for MIL-53(Al)-TDC.

amounts of confined H_2O have resulted in enhanced CO_2 capture[20]), under a constant N_2 flow (60 mL min^{-1}), and the change in the weight of the sample was recorded (see Fig. 2). Different relative humidities were explored (Fig. S3 and S4†) finding the optimal amount at 10%RH. When this weight change was constant (plateau, water confinement of 0.59 wt%), at 35 min, the N_2 flow was switched to a CO_2 flow (60 mL min^{-1}) and a sharp weight increase was observed (Fig. 2, bottom). Once the weight change was stable (plateau), the total CO_2 was equal to 6.5 wt% (Fig. 2, bottom). Thus, when confining small amounts of H_2O (0.59 wt%) within the micropores of MIL-53(Al)-TDC, the CO_2 capture was enhanced 1.3 times (from 5.0 to 6.5 CO_2 wt%). In comparison with some results previously performed in our group (confinement of water to improve CO_2 capture), such CO_2 capture enhancement for MIL-53(Al)-TDC was similar to other MOF functionalised systems with hydroxo groups.[20] For example, MIL-53(Al) was studied under the same flow conditions (as carried out in this work H_2O + CO_2), showing a CO_2 capture enhancement from 3.5 wt% under anhydrous conditions to 6.0 wt% when confining 0.5 wt% of water.[17b] Thus, the enhancement amount was proportional to the solvent amount (approximately 0.5 wt% of confined water).

Our research group is interested in confining other polar solvents (*vide supra*), within microporous MOFs to enhance their CO_2 capture capacities. Therefore, we decided to confine small amounts of EtOH inside the pores of MIL-53(Al)-TDC to investigate the resulting CO_2 adsorption properties. First, we investigated the EtOH adsorption properties of MIL-53(Al)-TDC.

Ethanol (EtOH) adsorption–desorption studies

Ethanol sorption experiments were carried out on the samples of MIL-53(Al)-TDC, and to the best of our knowledge, this is the first study which is presenting such experiments for this MOF material. First, an acetone-exchanged sample of MIL-53 (Al)-TDC was placed in an analyser cell and heated at 200 °C for 1 h and under a N_2 flow. When the sample was fully activated and cooled down to 30 °C, an EtOH adsorption–desorption isotherm was carried out from $\%P/P_0$ = 0 to 85 (Fig. 3).

From 0 to $10\%P/P_0$ the EtOH uptake rapidly increased due to the favourable host–guest interactions. At this point, an EtOH uptake of approximately 20 wt% (4.5 mmol g^{-1}) was achieved; Fig. 3. Then, from 10 to $85\%P/P_0$ a much slower (but constant) alcohol uptake was observed with a maximum uptake of approximately 32 wt% (6.5 mmol g^{-1}). A relatively strong hysteresis was observed in the desorption phase (Fig. 3, open symbols). This hysteresis occurred mainly in the low pressure range from 0 to $10\%P/P_0$. After the desorption phase was completed, some EtOH remained trapped inside the channels of this MOF material (19 wt%, 4.18 mmol g^{-1}) which indicated a strong affinity of MIL-53(Al)-TDC to EtOH. The pore dimensions of activated MIL-53(Al)-TDC are approximately 8.0 × 8.2 Å,[18] which are considerably much larger than the kinetic diameter of EtOH[21] (4.5 Å). Therefore, this observed hysteresis is mainly due to strong host–guest interactions between MIL-53(Al)-TDC and EtOH and are most likely due to the formation of relatively strong hydrogen bonds between the EtOH molecules and the bridging hydroxo functional groups (μ-OH), as corroborated by computational calculations (*vide infra*). In order to experimentally evaluate the "strength" of these interactions, another EtOH adsorption isotherm was carried out at 20 °C to calculate the isosteric heat of adsorption (ΔH_{ads}) for EtOH in MIL-53(Al)-TDC (fitting the two adsorption isotherms to the Clausius–Clapeyron equation, see the ESI†). The ΔH_{ads} value was estimated to be 69.6 kJ mol^{-1}, indicating a high EtOH affinity.

Later, an acetone-exchanged sample of MIL-53(Al)-TDC was activated (as previously described), cooled down to 30 °C (under N_2) and fully saturated with EtOH, by following an acti-

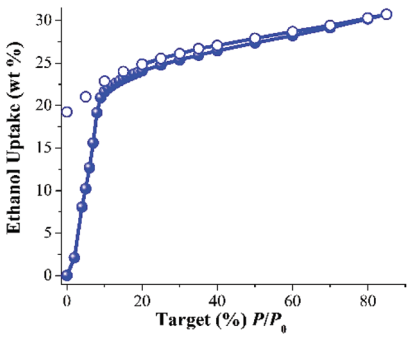

Fig. 3 Ethanol adsorption isotherm at 30 °C of MIL-53(Al)-TDC from $\%P/P_0$ = 0 to 85. Solid circles represent adsorption, and open circles show desorption.

vation protocol (see the ESI†). Thus, the residual amount of confined EtOH was equal to approximately 2 wt%. We decided to confine only small amounts of EtOH, in MIL-53(Al)-TDC, motivated by our previous experimental work on EtOH (2.6 wt%) confined within the micropores of InOF-1,[13] which led to a substantial improvement of the CO_2 capture (2.7 fold increase). To evaluate the reproducibility of the activation protocol for MIL-53(Al)-TDC, we performed 5 independent experiments, which provided us, approximately, the same confined amount of EtOH (2.08 wt%, see the ESI†). Hereinafter, this sample will be referred to as EtOH@ MIL-53(Al)-TDC.

Thus, a kinetic CO_2 adsorption experiment (30 °C) was performed on an EtOH@MIL-53(Al)-TDC sample. The total CO_2 capture was equal to 4.7 wt% (Fig. S5†). Since the CO_2 capture was not improved, we tested the confinement of different amounts of EtOH (1, 3 and 4 wt%), in activated samples of MIL-53(Al)-TDC, showing the same behaviour (no CO_2 capture enhancement, Fig. S5†). In order to understand this phenomenon, computational calculations were carried out.

Computational studies

To investigate the relationship between the presence of water and ethanol (confined inside MIL-53(Al)-TDC) and their affinity to CO_2, we have taken a simplified model of the binuclear [$Al_2(\mu_2$-OH)] building block (see Fig. 4) to computationally (geometry optimisations) describe molecular interactions. The binuclear building block contains the hydroxo functional group (μ_2-OH) which has been reported to be mainly responsible for the interactions (*via* hydrogen bonding) with H_2O and EtOH molecules in related frameworks.[13,20]

The computational investigation was focused on the hydrogen bond interactions[22] to confine H_2O and EtOH molecules and therefore, enhance the total capture CO_2. Optimised model structures for the binuclear [$Al_2(\mu_2$-OH)] building block with H_2O and EtOH molecules are shown in Fig. 5 and 6, emphasising their hydrogen bond distances and angles. First, the optimisation of the building block, H_2O and CO_2 is shown in Fig. 5 (left). The hydrogen bond between the H_2O molecule and CO_2 was approximately of 1.8 Å and a C═O···H angle close to 178.3°; Fig. 5 (left). Interestingly, when the optimised model is turned 90°, Fig. 5 (right), it is possible to observe the directionality of the hydrogen bond that positions the CO_2 molecule in the same plane as the H_2O molecule. In other words, once the μ_2-OH group is hydrogen bonded to a H_2O molecule, it can subsequently "pin" a CO_2 molecule in a straight line. Later, the optimised model with EtOH and CO_2 is shown in Fig. 6 (left). The hydrogen bond between the EtOH molecule and CO_2 was also close to 1.8 Å and the C═O···H angle was approximately 176.3°; Fig. 6 (left). When the model is rotated 90°, it is possible to see that EtOH and CO_2 are not in the same plane; Fig. 6 (right).

The overall result of these molecules being on the same plane (HOH···OCO) or out of the plane (EtOH···OCO) can be visualised in Fig. 7. The set HOH···OCO can be located inside the channel of MIL-53(Al)-TDC pointing towards the most favourable free space of the channel (see Fig. 7, left). In con-

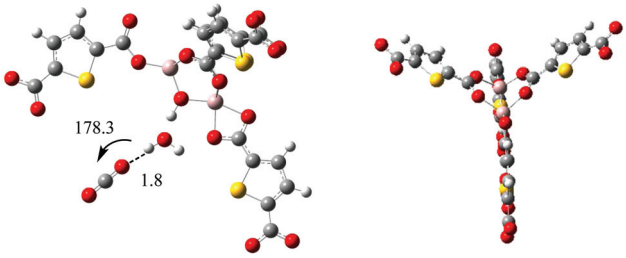

Fig. 5 Optimised structures of: (left) the binuclear [$Al_2(\mu_2$-OH)] building block model interacting with H_2O and CO_2, and (right) view of the same model rotated 90°.

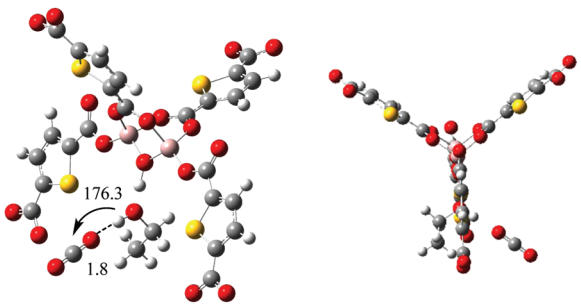

Fig. 6 Optimised structures of: (left) the binuclear [$Al_2(\mu_2$-OH)] building block model interacting with EtOH and CO_2, and (right) view of the same model rotated 90°.

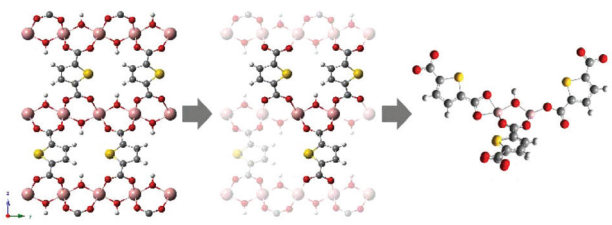

Fig. 4 Schematic representation of: (left) pore structure of MIL-53(Al)-TDC; (centre) section of the pore (model) that was taken to perform computational calculations and (right) the optimised structure of the binuclear [$Al_2(\mu_2$-OH)] building block model.

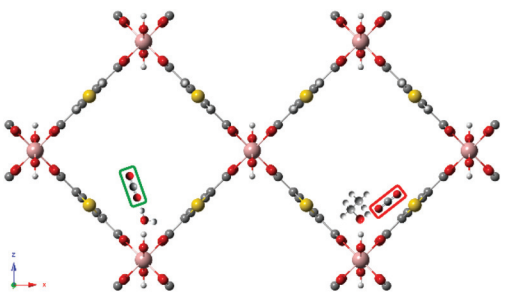

Fig. 7 Schematic representation of: (left) hydrogen bonded molecule set HOH···OCO and (right) hydrogen bonded molecule set EtOH···OCO inside the pore of MIL-53(Al)-TDC.

trast, the set EtOH···OCO is located in a less favourable position inside the channel of the material (see Fig. 7, right). The hydrogen bond between EtOH and CO_2, agglomerates such molecules around the μ_2-OH group and therefore, the free space in the channel is not efficiently used. These simple computational models provided us a plausible explanation to understand the CO_2 capture enhancement upon confining H_2O and the minimum variation on such capture when EtOH is confined.

In order to investigate more about these interactions (HOH···OCO and the set EtOH···OCO), the analysis of critical points of the electron density within the quantum theory of atoms in molecules (QTAIM)[23] is a very useful approach. Thus, critical points associated with hydrogen bonds can be classified according to the Hessian matrix eigenvalues, as other bond critical points, with the rank and signature (3,-1). To evaluate non-covalent interactions, the Non-Covalent-Index (NCI) isosurfaces were computed by the reduced density gradient coupled with the second eigenvalue of the Hessian matrix of the electron density.[24] The blue colour of the isosurface indicates that the interaction is attractive and strong (*i.e.*, mainly electrostatic); green colour represents weak interactions (van der Waals interactions); and red colour indicates strong and repulsive non-covalent interactions. The topological analysis of the electron density, including QTAIM and NCI, was carried out with GPUAM PROJECT v.1.0, a computational code which was previously developed in our group.[25] The wave function was computed from single point energy calculations of the optimised structures (*vide supra*), using Gaussian 09 software, at the B3LYP/6-31++G** level.

Fig. 8 shows the bond critical points in the frame of QTAIM and NCI isosurfaces of the model-structures with H_2O and EtOH, interacting with CO_2. Optimised structures are those previously calculated (Fig. 5 and 6). Table S1† presents the results of the QTAIM analysis (see the ESI†). Interestingly, the results for both systems are quite similar. The interaction of the [$Al_2(\mu_2$-OH)] model with H_2O and EtOH is partly covalent according to the ratio $-G(r)/V(r)$ and the negative value of $H(r)$.[26] However, in the [$Al_2(\mu_2$-OH)] and EtOH system, the negative value of the Laplacian indicated a more covalent character than for the [$Al_2(\mu_2$-OH)] and H_2O system (see Fig. 8). NCI corroborates these observations since there are no isosurfaces in the bond between [$Al_2(\mu_2$-OH)] and confined molecules (EtOH and H_2O). The interaction of both systems with CO_2 (either with H_2O or with EtOH) demonstrates the non-covalent character (the ratio $|G(r)/V(r)| > 1$ and positive $H(r)$), which according to the Popellier criteria,[27] can be classified as hydrogen bonds. The colour of the NCI isosurface indicates that the interaction with H_2O is more dispersive than with EtOH, being more electrostatic for EtOH (see Fig. 8, bottom). In the [$Al_2(\mu_2$-OH)] and EtOH system an extra S···O interaction (very weak) was found, which was absent for the[$Al_2(\mu_2$-OH)] and H_2O system. Finally, the interaction energy (E_{int}) was estimated by the Espinosa–Molins–Lecomte approximation.[28] In both systems, this interaction energy with CO_2 is similar and we can say that they are practically the same (see Table S1, ESI†).

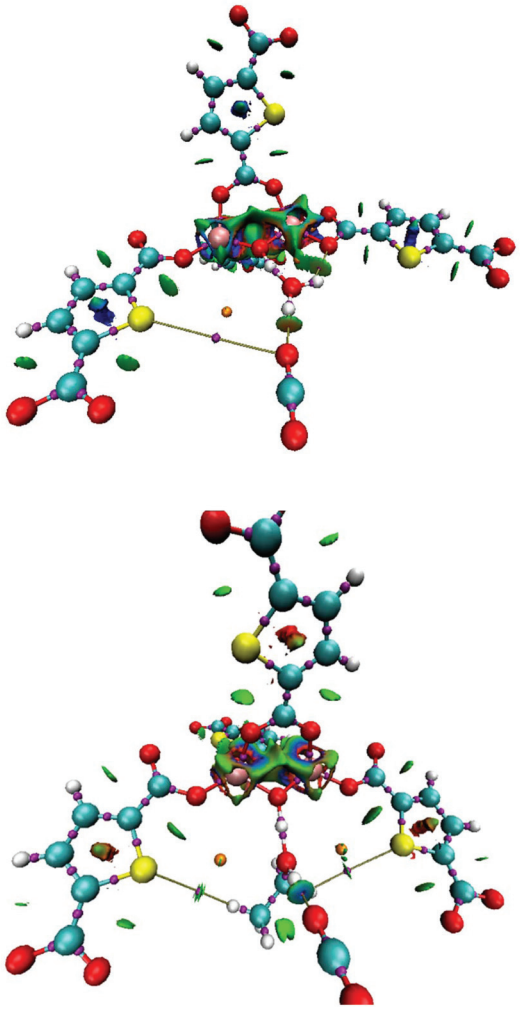

Fig. 8 Critical points and isosurfaces (no covalent interactions) of the binuclear [$Al_2(\mu_2$-OH)] building block model interacting with: (top) H_2O and CO_2 and (bottom) EtOH and CO_2. Bonding critical points (purple balls), ring critical points (orange balls) and bond paths (grey lines).

Therefore, these results corroborate that although both systems are very similar in terms of their non-covalent character, what determines the enhancement of the CO_2 capture is the location of these hydrogen bonds (critical points) inside the channel (Fig. 7).

Conclusions

Ethanol adsorption–desorption isotherms were, for the first time, investigated for the microporous MOF material MIL-53 (Al)-TDC. MIL-53(Al)-TDC showed, by kinetic isotherm CO_2 experiments, a total CO_2 uptake of 5.0 wt%. When confining small amounts of H_2O (0.59 wt%) within MIL-53(Al)-TDC, the CO_2 capture was enhanced 1.3 times (from 5.0 to 6.5 CO_2 wt%). Conversely, upon confining small amounts of EtOH (1.0, 2.0, 3.0 and 4.0 wt%) the total CO_2 captured was not improved.

Computational calculations provided us a plausible explanation to understand such CO_2 capture enhancement upon confining H_2O and, no CO_2 capture improvement when EtOH was confined. Distances and angles of the hydrogen bonds between the hydroxo functional group (μ_2-OH) and the confined molecules (H_2O and EtOH) were calculated to be very similar. However, the directionality of the hydrogen bond between confined molecules and CO_2 determined the overall CO_2 capture improvement. In addition, the presence of hydrogen bonds and their nature were corroborated by QTAIM and NCI. The hydrogen bond between H_2O and CO_2 was located in the most favourable free space of the channel.

Conflicts of interest

There are no conflicts to declare.

Acknowledgements

The authors thank Dr A. Tejeda-Cruz (X-ray; IIM-UNAM), PAPIIT UNAM Mexico (IN101517) and CONACyT (1789) for financial support. E.G.-Z. acknowledges CONACyT (236879), Mexico for financial support. D. S.-I. acknowledges PAPIIT UNAM Mexico (IA202418) and CONACyT (FC-2015-2/829) for funding. Thanks to U. Winnberg (ITAM) for scientific discussions. This work was carried out using a NES supercomputer, provided by Dirección General de Cómputo y Tecnologías de Información y Comunicación (DGTIC), Universidad Nacional Autónoma de México (UNAM), and the cluster Yoltla in the Laboratorio de Supercómputo y Visualización en Paralelo at the Universidad Autónoma Metropolitana-Iztapalapa. We would like to acknowledge the DGTIC of UNAM for its excellent and free supercomputing services. The authors would like to thank Oralia L Jiménez A., María Teresa Vázquez, Alberto López Vivas and Caín González for their technical support.

References

1 S. R. Batten, N. R. Champness, X.-M. Chen, J. Garcia-Martinez, S. Kitagawa, L. Öhrström, M. O'Keeffe, M. Paik Suh and J. Reedijk, *Pure Appl. Chem.*, 2013, **85**, 1715–1724.

2 J. Rogelj, G. Luderer, R. C. Pietzcker, E. Kriegler, M. Schaeffer, V. Krey and K. Riahi, *Nat. Clim. Change*, 2015, **5**, 519–527.

3 (*a*) G. P. Peters, C. Le Quéré, R. M. Andrew, J. G. Canadell, P. Friedlingstein, T. Ilyina, R. B. Jackson, F. Joos, J. I. Korsbakken, G. A. Mckinley, S. Sitch and P. Tans, *Nat. Clim. Change*, 2017, **7**, 848–852; (*b*) R. B. Jackson, C. Le Quéré, R. M. Andrew, J. G. Canadell, G. P. Peters, J. Roy and L. Wu, *Environ. Res. Lett.*, 2017, **12**, 110202.

4 M. Poliakoff, W. Leitner and E. S. Streng, *Faraday Discuss.*, 2015, **183**, 9–17.

5 Y. H. Choi, Y. J. Jang, H. Park, W. Y. Kim, Y. H. Lee, S. H. Choi and J. S. Lee, *Appl. Catal., B*, 2017, **202**, 605–610.

6 K. Sumida, D. L. Rogow, J. A. Mason, T. M. McDonald, E. D. Bloch, Z. R. Herm, T. H. Bae and J. R. Long, *Chem. Rev.*, 2012, **112**, 724–781.

7 P. Pachfule and R. Banerjee, *Cryst. Growth Des.*, 2011, **11**, 5176–5181.

8 M. Dincă and J. R. Long, *Angew. Chem., Int. Ed.*, 2008, **47**, 6766–6779.

9 A. Luzar and D. Bratko, *J. Phys. Chem. B*, 2005, **109**, 22545–22552.

10 E. Soubeyrand-Lenoir, C. Vagner, J. W. Yoon, P. Bazin, F. Ragon, Y. K. Hwang, C. Serre, J. S. Chang and P. L. Llewellyn, *J. Am. Chem. Soc.*, 2012, **134**, 10174–10181.

11 N. C. Burtch, H. Jasuja and K. S. Walton, *Chem. Rev.*, 2014, **114**, 10575–10612.

12 J. Qian, J. Shen, Q. Li, Y. Hu and S. Huang, *CrystEngComm*, 2017, **19**, 5346–5350.

13 R. A. Peralta, A. Campos-Reales-Pineda, H. Pfeiffer, J. R. Alvarez, J. A. Zárate, J. Balmaseda, E. González-Zamora, A. Martínez, D. Martínez-Otero, V. Jancik and I. A. Ibarra, *Chem. Commun.*, 2016, **52**, 10273–10276.

14 E. Sánchez-González, E. González-Zamora, D. Martínez-Otero, V. Jancik and I. A. Ibarra, *Inorg. Chem.*, 2017, **56**, 5863–5872.

15 (*a*) E. Sánchez-González, P. G. M. Mileo, J. R. Álvarez, E. González-Zamora, G. Maurin and I. A. Ibarra, *Dalton Trans.*, 2017, **46**, 15208–15215; (*b*) G. A. González-Martínez, J. A. Zárate, A. Martínez, E. Sánchez-González, J. R. Álvarez, E. Lima, E. González-Zamora and I. A. Ibarra, *RSC Adv.*, 2017, **7**, 24833–24840.

16 J. Raziel Alvarez, P. G. M. Mileo, E. Sánchez-González, J. A. Zarate, J. Rodriguez-Hernandez, E. González-Zamora, G. Maurin and I. A. Ibarra, *J. Phys. Chem. C*, 2018, **122**, 5566–5577.

17 (*a*) M. Sánchez-Serratos, P. A. Bayliss, R. A. Peralta, E. González-Zamora, E. Lima and I. A. Ibarra, *New J. Chem.*, 2016, **40**, 68–72; (*b*) A. Zárate, R. A. Peralta, P. A. Bayliss, R. Howie, M. Sánchez-Serratos, P. Carmona-Monroy, D. Solis-Ibarra, E. González-Zamora and I. A. Ibarra, *RSC Adv.*, 2016, **6**, 9978–9983; (*c*) E. Sánchez-González, J. R. Álvarez, R. A. Peralta, A. Campos-Reales-Pineda, A. Tejeda-Cruz, E. Lima, J. Balmaseda, E. González-Zamora and I. A. Ibarra, *ACS Omega*, 2016, **1**, 305–310; (*d*) J. R. Álvarez, R. A. Peralta, J. Balmaseda, E. González-Zamora and I. A. Ibarra, *Inorg. Chem. Front.*, 2015, **2**, 1080–1084.

18 C. B. L. Tschense, N. Reimer, C. W. Hsu, H. Reinsch, R. Siegel, W. J. Chen, C. H. Lin, A. Cadiau, C. Serre, J. Senker and N. Stock, *Z. Anorg. Allg. Chem.*, 2017, **643**, 1600–1608.

19 T. Loiseau, C. Serre, C. Huguenard, G. Fink, F. Taulelle, M. Henry, T. Bataille and G. Férey, *Chem. – Eur. J.*, 2004, **10**, 1373–1382.

20 E. González-Zamora and I. A. Ibarra, *Mater. Chem. Front.*, 2017, **1**, 1471–1484.

21 T. Borjigin, F. Sun, J. Zhang, K. Cai, H. Ren and G. Zhu, *Chem. Commun.*, 2012, **48**, 7613–7615.
22 (*a*) J. Z. Ramírez, R. Vargas and J. Garza, *J. Mex. Chem. Soc.*, 2008, **52**, 31–35; (*b*) R. Vargas, J. Garza, D. A. Dixon and B. P. Hay, *J. Am. Chem. Soc*, 2000, **122**, 4750–4755.
23 R. F. W. Bader, *Atoms in Molecules: A Quantum Theory*, Oxford University, New York, 1990.
24 (*a*) E. R. Johnson, S. Keinan, P. Mori-Sanchez, J. Contreras-Garcia, A. J. Cohen and W. Yang, *J. Am. Chem. Soc.*, 2010, **132**, 6498–6506; (*b*) J. Contreras-Garcia, E. R. Johnson, S. Keinan, R. Chaudret, J. P. Piquemal, D. N. Beratan and W. Yang, *J. Chem. Theory Comput.*, 2011, **7**, 625–632.
25 R. Hernández-Esparza, S. M. Mejía-Chica, A. D. Zapata-Escobar, A. Guevara-García, A. Martínez-Melchor, J. M. Hernández-Pérez, R. Vargas and J. Garza, *J. Comput. Chem.*, 2014, **35**, 2272–2278.
26 P. S. V. Kumar, V. Raghavendra and V. Subramanian, *J. Chem. Sci.*, 2016, **128**, 1527–1536.
27 (*a*) E. Cubero, M. Orozco, P. Hobza and F. J. Luque, *J. Phys. Chem. A*, 1999, **103**, 6394–6401; (*b*) P. Hobza, J. Sponer, E. Cubero, M. Orozco and F. J. Luque, *J. Phys. Chem. B*, 2000, **104**, 6286–6292.
28 E. Espinosa, E. Molins and C. Lecomte, *Chem. Phys. Lett.*, 1998, **285**, 170–173.